Inhibition of Histone H3K27 Demethylases Inactivates Brachyury (TBXT) and Promotes Chordoma Cell Death

Lucia Cottone[1], Adam P. Cribbs[2], Garima Khandelwal[3], Graham Wells[2], Lorena Ligammari[1], Martin Philpott[2], Anthony Tumber[4], Patrick Lombard[1], Edward S. Hookway[1,2], Tamas Szommer[4], Catrine Johansson[2], Paul E. Brennan[4], Nischalan Pillay[1,5], Richard G. Jenner[3], Udo Oppermann[2,4,6], and Adrienne M. Flanagan[1,5]

ABSTRACT

Expression of the transcription factor brachyury (TBXT) is normally restricted to the embryo, and its silencing is epigenetically regulated. TBXT promotes mesenchymal transition in a subset of common carcinomas, and in chordoma, a rare cancer showing notochordal differentiation, TBXT acts as a putative oncogene. We hypothesized that TBXT expression is controlled through epigenetic inhibition to promote chordoma cell death. Screening of five human chordoma cell lines revealed that pharmacologic inhibition of the histone 3 lysine 27 demethylases KDM6A (UTX) and KDM6B (JMJD3) leads to cell death. This effect was phenocopied by dual genetic inactivation of KDM6A/B using CRISPR/Cas9. Inhibition of KDM6A/B with a novel compound KDOBA67 led to a genome-wide increase in repressive H3K27me3 marks with concomitant reduction in active H3K27ac, H3K9ac, and H3K4me3 marks. *TBXT* was a KDM6A/B target gene, and chromatin changes at *TBXT* following KDOBA67 treatment were associated with a reduction in TBXT protein levels in all models tested, including primary patient-derived cultures. In all models tested, KDOBA67 treatment downregulated expression of a network of transcription factors critical for chordoma survival and upregulated pathways dominated by ATF4-driven stress and proapoptotic responses. Blocking the AFT4 stress response did not prevent suppression of TBXT and induction of cell death, but ectopic overexpression of *TBXT* increased viability, therefore implicating TBXT as a potential therapeutic target of H3K27 demethylase inhibitors in chordoma. Our work highlights how knowledge of normal processes in fetal development can provide insight into tumorigenesis and identify novel therapeutic approaches.

Significance: Pharmacologic inhibition of H3K27-demethylases in human chordoma cells promotes epigenetic silencing of oncogenic TBXT, alters gene networks critical to survival, and represents a potential novel therapy.

Introduction

Normal embryonic development requires a finely coordinated process of temporal and spatial gene expression that is controlled through epigenetic mechanisms (1, 2). In addition, aberrant epigenetic mechanisms also have been implicated in the pathogenesis of a diverse range of malignancies (3). During vertebrate development, mesoderm specification is tightly regulated by the prototypical T-box transcription factor T (TBXT, also known as T, or brachyury). *TBXT* expression is exquisitely orchestrated through caudo-cranial morphogenic gradients, controlled through fibroblast growth factor and activin signaling, and ultimately transforms the nascent dorsal mesoderm into the rudimentary axial skeleton, the notochord (4, 5). *TBXT* is silenced in the human fetus at approximately 12 weeks of development, and consequently, the notochord recedes prenatally (6).

In embryonic stem cells, and mesoderm-derived differentiating adipocytes, regulation of *TBXT* gene expression is achieved through epigenetic regulatory mechanisms. These include the recruitment of histone deacetylase 1 (HDAC1; ref. 7), CpG island methylation (8, 9), and the action of histone lysine demethylases, in particular lysine demethylase 6A [KDM6A, also known as ubiquitously transcribed X chromosome tetratricopeptide repeat protein (UTX)] and lysine demethylase 6B [KDM6B, Jumonji domain containing 3 (JMJD3); hereafter referred to as KDM6A/B; refs. 10, 11], which act on trimethylated histone H3 lysine 27 (H3K27me3). H3K27me3 marks are deposited by polycomb repressive complex 2 (PRC2), inhibit H3K27 acetylation (12, 13), and recruit the canonical form of polycomb repressive complex 1 (PRC1) to maintain developmental regulator genes in a repressed state (14, 15).

TBXT expression is seen in chordoma, a rare cancer of the axial skeleton showing notochordal differentiation, in the benign notochordal cell tumor, the postulated precursor of chordoma, and in hemangioblastoma (16, 17). Lower levels of *TBXT* are also detected in a proportion of tumors of epithelial origin (lung, prostate, and breast cancer), where TBXT promotes tumor progression and epithelial–mesenchymal transition (18). TBXT is expressed at high levels in

[1]Department of Pathology, UCL Cancer Institute, University College London, London, United Kingdom. [2]Botnar Research Centre, Nuffield Department of Orthopaedics, Rheumatology and Musculoskeletal Sciences, University of Oxford, Oxford, United Kingdom. [3]Department of Cancer Biology, UCL Cancer Institute, University College London, London, United Kingdom. [4]Structural Genomics Consortium, University of Oxford, Oxford, United Kingdom. [5]Department of Histopathology, Royal National Orthopaedic Hospital, Stanmore, Middlesex, United Kingdom. [6]FRIAS - Freiburg Institute of Advanced Studies, University of Freiburg, Freiburg, Germany.

Note: Supplementary data for this article are available at Cancer Research Online (http://cancerres.aacrjournals.org/).

A.M. Flanagan and U. Oppermann contributed equally to this article.

Corresponding Authors: Adrienne M. Flanagan, University College London, London WC1E 6BT, United Kingdom. Phone: 44-0-20-7679-6304; E-mail: a.flanagan@ucl.ac.uk; and Udo Oppermann, Botnar Research Centre, Old Rd, Headington, Oxford OX3 7LD, United Kingdom. Phone: 44-0-1865-227308; E-mail: udo.oppermann@sgc.ox.ac.uk

Cancer Res 2020;80:4540–51

doi: 10.1158/0008-5472.CAN-20-1387

chordomas (19), and several lines of evidence demonstrate that it plays a pivotal role in the development of this disease (20); namely germline tandem duplication of *TBXT* is associated with familial chordoma (21) and similar somatic changes are seen in sporadic tumors (22). Furthermore, TBXT regulates an oncogenic transcriptional network (20), silencing of which causes growth arrest in chordoma cell lines (23, 24). However, the key mechanism(s) that regulate the expression of *TBXT* in chordoma have not been reported and cannot be accounted for solely by somatic copy-number gains, which are observed only in up to 27% of sporadic cases (22). Hence, we postulated that persistent expression of *TBXT* in chordoma results from disruption of the physiologic epigenetic process(es) that control its expression in development, and that such pathways could be exploited for targeted therapy.

An increasing number of therapeutic approaches targeting epigenetic pathways have shown promising results in cancer, for example in acute myeloid leukemia (25), multiple myeloma (26), brain tumors (27), and neuroblastoma (28). More recently, chordoma has been added to this list, with experiments revealing an association of *TBXT* with an active superenhancer, which can be therapeutically exploited by inhibiting cyclin-dependent kinases with roles in transcriptional regulation, such as CDK7/12/13, via downregulation of *TBXT* expression (29).

Individuals with chordoma have a median of 7-year survival, and they have seen little benefit from genomic investigations seeking tractable therapeutic targets such as protein kinases (22). Herein, we used a focused library of mechanistically defined epigenetic inhibitor tool compounds with the aim of identifying vulnerable signaling pathways that could be exploited for the development of novel treatments for chordoma.

Materials and Methods

Cell lines and primary cultures

Five human chordoma cell lines, U-CH1, U-CH2, U-CH7, MUG-Chor, and UM-Chor, were cultured as described previously (30). All chordoma cell lines derive from sacral tumors except UM-Chor, which was generated from a clival chordoma (www.chordomafoundation.org). U2OS (ATCC HTB96, ATCC), an osteosarcoma cell line that lacked expression of TBXT was used as a control and was cultured according to ATCC guidelines. Cells lines were quality controlled by short-tandem-repeat analysis (DNA Diagnostic Centre; last report in Supplementary Table S1) and were tested regularly to ensure that they were mycoplasma-free.

Fresh sacral chordoma samples were obtained with written-informed consent from patients being treated at the Royal National Orthopaedic Hospital (RNOH), Stanmore, United Kingdom. Tumor diagnoses were made according to the World Health Organization classification (16). Human investigations were performed after approval by an Institutional Review Board: ethical approval was obtained from the Cambridgeshire 2 Research Ethics Service (reference 09/H0308/165). The studies were conducted in accordance with the Declaration of Helsinki ethical guidelines. Fresh chordoma samples were obtained within 30 minutes of being removed from the patient; the samples were washed in PBS supplemented with antibiotics (Primocin, 100 μg/mL, Invivogen), minced, and incubated with Collagenase II (100 mg/mL, 17101–015, Thermo Fisher Scientific) for 1 hour. The digested tissue samples were then passed through a 70 μm cell strainer, centrifuged, and then resuspended in chordoma medium (as described in ref. 30). On reaching confluence, cells were passaged once and then plated at equal density for KDOBA67 treatment. The assay was repeated with four independent donors, each with at least three biological replicates.

Screening of small-molecule inhibitors, compound synthesis, and compound treatments

To screen small-molecules inhibitors, human chordoma cell lines (U-CH1, U-CH2, U-CH7, MUG-Chor, and UM-Chor) were seeded at a density of 5,000 cells per well in a 96-well plate overnight. Cells were treated with either a compound or vehicle control (0.1% DMSO) for 3 to 6 days (a list of compounds and concentrations used is available in Supplementary Dataset S1). Cell viability was measured using Presto Blue Cell Viability Reagent (Thermo Fisher Scientific). Viability was normalized to vehicle controls within the same plate. Each assay was repeated 3 times, using 3 replicates and the mean decrease in viability calculated. For IC_{50} determination, cells were plated as above and treated with halving the dilution of the compounds with the highest concentration being 50 μmol/L. Viability was measured by Presto Blue Cell Viability Reagent (Thermo Fisher Scientific) as above. IC_{50} was calculated by fitting 7-point dose–response data using Prism version 5. Quoted values represent the mean of three independent experiments, each with three replicates.

In follow-up experiments, chordoma cell lines were treated with compounds at the IC_{80}: GSK-J4 (5 μmol/L, Cayman Chemicals), KDOBA67 (5 μmol/L), and ISRIB (250 nmol/L, Sigma Aldrich) for 48 hours (or for 72 hours in apoptosis and cell-cycle experiments only) unless otherwise specified. Primary chordoma cultures were treated with KDOBA67 (10 μmol/L) for 6 days. DMSO was used at the same concentration as vehicle control (0.1%).

Detailed methods regarding the synthesis of the KDOBA67 compound, IC_{50} determination of GSK-J1 analogs, and structure determination of UTY in complex with KDOBA67 (protein crystallization, X-ray data collection, and structure determination) are available in Supplementary Materials and Methods, Supplementary Fig. S1A–S1C, and Supplementary Tables S2 and S3.

Apoptosis and cell-cycle studies

Experiments were performed on an LSR Fortessa (Becton Dickinson) running FACSDiva Software version 6 with 10^4 events recorded for each sample.

Cell-cycle analysis

Propidium iodide (PI) staining. Subconfluent cultures of cells were treated with compounds at the IC_{50} concentration between 47 and 72 hours. Cells were harvested, washed once in PBS (Thermo Fisher Scientific), and counted. Note that 2×10^5 cells were fixed in 70% ethanol in PBS on ice for 30 minutes. Fixed cells were centrifuged at 3,000 rpm for 5 minutes and washed with PBS. To ensure that only DNA was stained, the pellet was treated with ribonuclease A (100 μg/mL in PBS, Thermo Fisher Scientific) and subsequently stained with PI solution in PBS (50 μg/mL, Sigma-Aldrich) at room temperature in the dark for 30 minutes prior to analysis.

Apoptosis detection

Apoptosis was determined by detecting phosphatidylserine by allophycocyanin (APC)-conjugated Annexin V using the APC Annexin V Apoptosis Detection Kit with PI (Biolegend). Briefly, following compound treatment as above, cells were harvested and washed once in PBS, and 2×10^5 cells were resuspended in 250 μL of binding buffer containing 5 μL Annexin V–APC and 10 μL PI solution. Cells were incubated in the dark for 15 minutes before being analyzed. Each assay was repeated 3 times, each with 3 replicates.

Western blotting, qPCR, and immunofluorescence

Western blotting and qPCRs were performed as described previously (30). Antibodies and primers are listed in Supplementary Tables S4 and S5, respectively. For the analysis of the nascent unprocessed RNA, equal amounts of total RNA were retrotranscribed using the Superscript-IV RT cDNA synthesis Kit (Thermo Scientific), and qPCR was carried out using specific primers designed to amplify the first intronic regions of the transcript of interest. No amplification was observed in control reactions lacking reverse transcriptase.

Immunofluorescence of primary chordoma cells was performed as described previously (31) using antibodies listed in Supplementary Table S4.

CRISPR/Cas9 knockdown

Target guide sequences validated against *KDM6A, KDM6B*, and *TBXT* were designed as previously published (cf. Supplementary Table S5). Guides were cloned in a CRISPR/Cas9 lentiviral backbone containing a puromycin and a blasticidin resistance cassette, respectively, as described previously (32). LentiCRISPR v2-Blast (Addgene plasmid # 83480) was a gift from Mohan Babu (University of Regina, Saskatchewan, Canada). LentiCRISPR v2 (Addgene plasmid # 52961) was a gift from Feng Zhang (Massachusetts Institute of Technology, Cambridge, MA). The empty vectors were used as a nontargeting control. Lentiviral particles were produced as described previously (31). Chordoma cells were transduced with a multiplicity of infection (MOI) of 1 and subjected to antibiotic selection (puromycin, sc-108071, Insight Biotechnology Ltd., at 2 μg/mL for UCH1 and UM-Chor, 4 μg/mL for MUG-Chor and blasticidin, A1113903, Thermo Fisher Scientific, at 10 μg/mL for UCH1 and UM-Chor, 20 μg/mL for MUG-Chor) using constructs in a sequential manner. Each knockout experiment was repeated twice for each of three chordoma cell lines, with at least four replicates per condition per assay. Genome targeting efficiency was assessed in a cleavage assay using the T7 Endonuclease I according to the manufacturer's instructions (M0302, New England Biolabs) or by Sanger Sequencing of PCR-amplified DNA of targeted cells. Cell proliferation was assessed 72 hours after the transduction of the second CRISPR construct by Presto Blue Viability Assay (Thermo Fisher Scientific) according to the manufacturer's instruction. Each assay was repeated twice using at least five replicates. Viability was normalized to vehicle controls within the same plate.

TBXT overexpression

The sequence of the *TBXT* transcript (TBXT-201 ENST-00000296946.6, Ensembl) corrected for the G177D variant and in frame to an HA-tag was cloned into a pHIV-dTomato lentiviral vector (a gift from Bryan Welm, Addgene plasmid # 21374), as described in Supplementary Fig. S7K. The empty vector was used as control (EV). Lentiviral particles were produced as described previously (31). Chordoma cells were seeded on 96-well collagen-coated plates and transduced with an MOI of 10 with the addition of Polybrene 5 μg/mL, which gave a positivity of infection of >95% as assessed by the expression of dTomato 72 hours after infection. UCH1 cells were treated with 5 μmol/L KDOBA67 and cell proliferation assessed as described above. For Western blot, cells were seeded in collagen-coated 6-well plates.

Chromatin immunoprecipitation, ChIP-Rx, and library preparation

Chromatin immunoprecipitation (ChIP) was performed as described in Supplementary Materials and Methods. ChIP-Rx was performed as ChIP with the exception that a fixed ratio of *Drosophila* S2 cells (20% of chordoma cells) was spiked in prior to fixation to allow for normalization. Libraries were prepared using the NEBNext Ultra 2 DNA Library Preparation Kit (New England Biolabs) and sequenced on a Nextseq500 (Illumina).

RNA sequencing library preparation

Cells were lysed in TRIzol and total RNA extracted using the Direct-zol Kit (Zymo Research) including an on-column DNA digest. Poly(A) RNA was selected using the NEBNext Poly(A) mRNA Magnetic Isolation Module (New England Biolabs) and a first-strand library prepared using NEBNext Ultra Directional RNA Library Prep Kit (New England Biolabs) and sequenced on a Nextseq 500 (Illumina).

Next-generation sequencing data processing

Computational pipelines were used by calling scripts from the CGAT toolkit to analyze the next-generation sequencing data (https://github.com/cgat-developers; ref. 33).

RNA-seq

Briefly, FASTQ files were assessed for quality using FASTQC, aligned to GRCh37 and a concatenated genome consisting of GRCh37 using the default options of HISAT2 (34). Differential gene expression analysis was performed using DESeq2 using cell type and treatment as factors in the model. Genes were considered to be differentially regulated based on $\log_2$-fold change and P value < 0.05. A list of genes differentially expressed in response to KDOBA67 is provided in Supplementary Dataset S2.

ChIP-Rx

ChIP-Rx data were aligned to a concatenated genome sequence of human (GRCh37-hg19) and spike-in of *Drosophila* (BDGP5.25) using bowtie2 (35) with very-sensitive option. Only uniquely mapped reads and properly paired reads (for paired-end data) were used for the downstream analysis. PCR duplicates were removed using samtools (http://www.htslib.org/). The peak calling was performed using SICER (FDR = 0.05; ref. 36) and filtered for blacklisted regions in the human genome. Peaks present in all the replicates in each condition (control and treatment) of a histone mark were used for further analysis. A peak set was created from the merged peaks between the two conditions and used for differential binding analysis for each histone mark. Read counts were obtained for individual replicates for the peak set using DiffBind, and differential binding analysis was performed using DESeq2 in R. Spike-in calibration for differential binding analysis was performed utilizing methods described in ref. 37. The metaplots and heatmaps were generated with computeMatrix and plotProfile/plotHeatmap functions from deeptools (https://deeptools.readthedocs.io/en/develop/). Genome coverage tracks were obtained using MACS2 pileup function (38) and visualized with Gviz and biomaRt in R. Differentially bound H3K27me3 peaks were overlapped with ± 1Kb of the transcription start sites (TSS); genes with a $\log_2$-fold change >1.25 were used for enrichment analysis using gprofiler2 in R.

DNA methylation analysis

DNA was extracted from either formalin-fixed paraffin-embedded or fresh-frozen tumors using QIAamp DNA Kits (Qiagen) according to the manufacturer's instructions. Between 0.5 and 1 μg DNA was used for the Infinium Methylation EPIC array or 450K Infinium Human Methylation array (Illumina). Data were assembled using BeadStudio (Illumina) and processed using Minfi[1] employing the

functional normalization protocol. Beta values were downloaded from the Cancer Genome Atlas for cancers other than chordoma.

Statistical analysis

Statistical parameters including the exact value of *n*, precision measures (mean ± SD), and statistical significance are reported in the figures. Data were judged to be statistically significant when $P < 0.05$ by two-tailed Student *t* test performed in GraphPad PRISM 5.0; asterisks denote statistical significance as calculated by Student *t* test (*, $P \le 0.05$; **, $P \le 0.01$; ***, $P \le 0.001$; and ****, $P \le 0.0001$).

Definition of experimental replicates

"Independent experiment" refers to an experiment that has been performed multiple times (e.g., the same experiment was performed on different days, using different primary patient samples). "Replicates" refers to biological replicates and represents multiple tests within the same experiment (i.e., multiple wells exposed to the drug). "Technical repeats" of the same replicate (e.g., multiple qPCR reads of the same replicate) have been averaged and are not used as independent values in the statistical analysis.

Data availability

Data are deposited in the National Center for Biotechnology Information GEO database: RNA-seq and ChIP-Rx sequencing experiments under accession number GSE120214, DNA methylation array data under accession number GSE119462.

Coordinates and structure factors for the UTY:KDOBA67 ligand complex are deposited with RCSB under PDB ID 5A1L.

Results

Inhibition of H3K27 demethylases reduces chordoma cell viability

We screened a library of tool compounds targeting proteins involved in chromatin biology including epigenetic readers, writers, and erasers, against five chordoma cell lines (www.chordomafounda

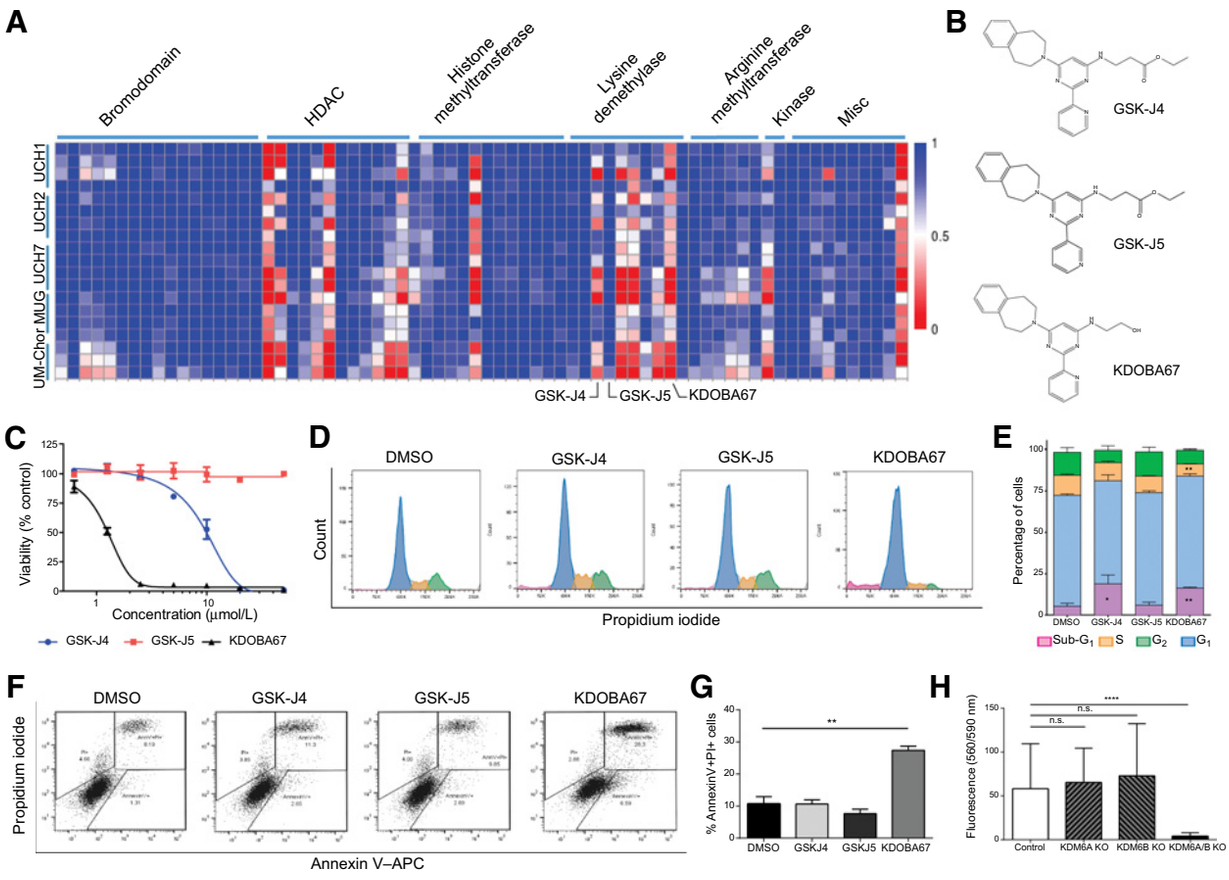

Figure 1.

Focused epigenetic library screening identifies H3K27 lysine demethylases as potential therapeutic target in chordoma. **A,** Screening of 90 small-molecule probes with validated activity against enzymes involved in chromatin biology on 5 chordoma cell lines. Each row represents a separate replicate and each column an individual compound. Columns have been grouped together by inhibitor class (cf. also to Supplementary Dataset S1). Values plotted as fractional viability compared with vehicle (DMSO) control. **B,** Molecular structures of GSK-J4, GSK-J5, and KDOBA67. **C,** Dose–response curves for GSK-J4, GSK-J5, and KDOBA67 in UM-Chor. **D–G,** Cell-cycle changes (**D** and **E**) and cell death analysis assessed by Annexin V–PI staining (**F** and **G**) in response to the compounds after 72 hours of treatment. Representative histogram/dot plots and quantification of three independent experiments, with three replicates per condition (cf. also Supplementary Fig. S2). **H,** Viability measured by Alamar blue of UCH1 following CRISPR/Cas9 editing of *KDM6A/B* or both. Mean of two independent experiments, with at least 6 replicates per condition per experiment. *, $P \le 0.05$; **, $P \le 0.01$; ****, $P \le 0.0001$; n.s., nonsignificant.

tion.com; Supplementary Dataset S1; ref. 39). A resazurin-based viability assay was used as the primary antiproliferative readout (**Fig. 1A**). Decreased cell viability was observed in all cell lines in response to HDAC inhibitors, as previously reported (40). Broad-spectrum inhibitors of the Jumonji-type of lysine demethylases were found to reduce cell viability, as was the more specific inhibitor of KDM6A/B GSK-J4 (**Fig. 1A** and **B**; ref. 41). Decreased viability was also observed with KDOBA67, a novel cell-permeable hydroxyl derivative of GSK-J4, which unlike its parental compound does not require activation by intracellular esterases (**Fig. 1A** and **B**; Supplementary Fig. S1A–S1C). KDOBA67 displayed *in vitro* inhibitory activity in the low micromolar range with IC_{50} values of 2 to 5 μmol/L in various chordoma cell lines (**Fig. 1C**) leading to induction of apoptosis (**Fig. 1D–G**; Supplementary Fig. S2A–S2F). As expected, the regioisomer control compound GSK-J5 did not display antiproliferative effects (**Fig. 1A–G**; Supplementary Fig. S2A–S2F).

To confirm that the inhibitory growth effects with the tool compounds were due to on-target inhibition of KDM6A/B, we used CRIPSR/Cas9 to introduce nonsense mutations in both genes (Supplementary Fig. S3A and S3B). Targeting *KDM6A/B* independently in UCH1 and UM-Chor cells, in which both genes are intact, was insufficient to reduce cell viability, whereas editing both genes simultaneously resulted in reduction in cell viability and proliferation (**Fig. 1H**; Supplementary Fig. S3C–S3E). The on-target effect was further supported by the reduction in viability following inactivation of *KDM6A* only in the MUG-Chor cell line, which contains a biallelic deletion of *KDM6B* (Supplementary Fig. S3F–S3H).

Inhibition of H3K27 demethylases targets critical pathways for chordoma cell survival

The transcriptional profile of the chordoma cell lines UCH1, UCH7, MUG-Chor, and UM-Chor (Supplementary Dataset S2 and Supplementary Fig. S4A–S4E) treated with inhibitors of KDM6A/B revealed significant changes in gene expression (**Fig. 2A** and **B**). Alteration in the expression of 371 genes was identified across all chordoma cell lines, and the affected pathways were linked to chordoma biology (20), and relate to cell movement, adhesion, extracellular matrix organization, cell contact, and signaling (**Fig. 2C**). This analysis also revealed enrichment in categories such as apoptosis, mitochondrial impairment, cell cycle arrest, and mitosis with identification of key genes such as aurora kinase A (*AURK),* dual-specific phosphatase 10 *(DUSP10),* activating transcription factor 4 (*ATF4*), DNA damage inducible transcript 3 (*DDIT3),* and the ATF4/DDIT3-target gene ChaC glutathione

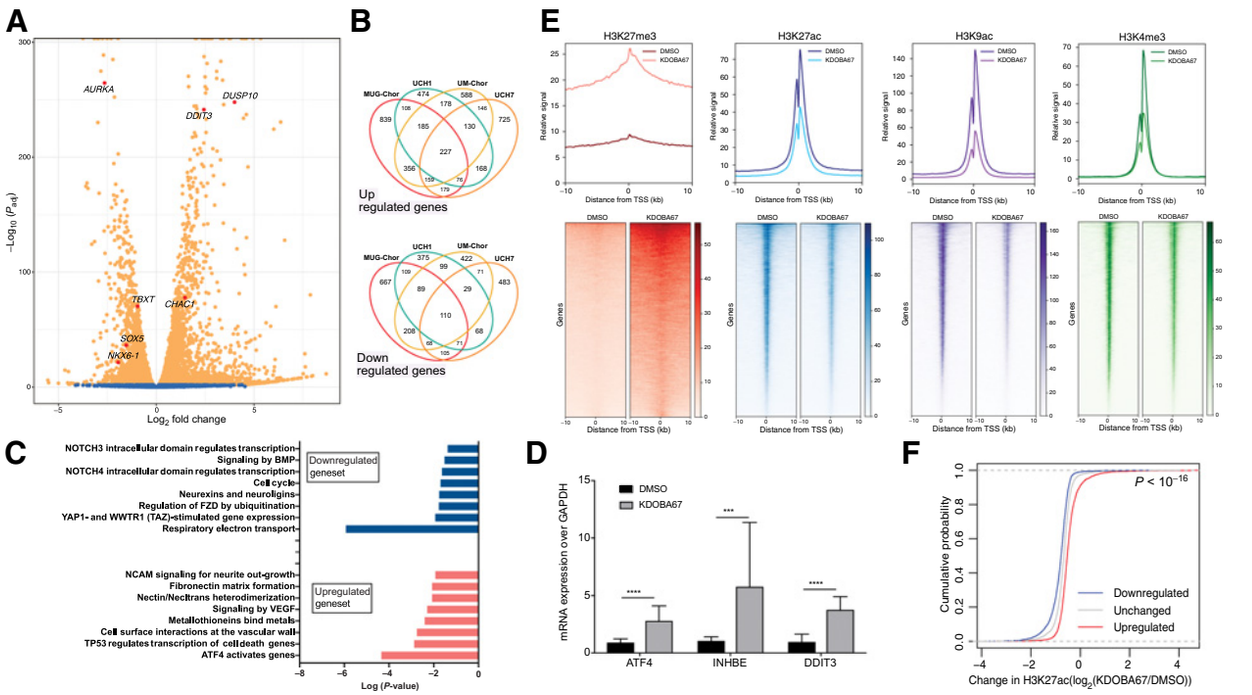

Figure 2.

Epigenomic and transcriptomic profiling in response to H3K27 lysine demethylase inhibitors in chordoma cell lines. **A,** Volcano plot summarizing differential gene expression in chordoma cells (UM-Chor) following treatment with KDOBA67 for 48 hours. Blue, not significant; orange, adjusted *P* value (P_{adj}) < 0.05. Average of three biological replicates. Results for UCH1, MUG-Chor, and UCH7 in Supplementary Fig. S4 and Supplementary Dataset S2. *TBXT* expression was reduced across chordoma cell lines [log_2-fold changes -2.1 (MUG-Chor), -1.2 (UCH1), -0.96 (UM-Chor), -1.5 (UCH7; $P_{adj} < 0.01$)]. **B,** Venn diagrams showing the numbers of upregulated (top) and downregulated (bottom) genes in four chordoma cell lines, an average of three biological replicates per cell line. **C,** Reactome analysis for UCH1, UCH7, UM-Chor, and MUG-Chor in response to KDOBA67. **D,** Upregulation of *ATF4* and ATF4-target genes (inhibin subunit beta E, *INHBE* and *DDIT3*) in patient-derived primary chordoma cultures as assessed by qPCR (four independent primary samples, at least three biological replicates per condition). **E,** Metagene plots (top) and heatmaps (bottom) of ChIP-Rx peaks of H3K27me3, H3K27ac, H3K9ac, and H3K4me3 in UCH1 cells treated with KDOBA67 or DMSO treatment for 48 hours. The signal represents the average of two or three biological replicates per condition. Principal component analysis plots of single replicates are shown in Supplementary Fig. S4F, S4H–S4J. **F,** Cumulative distribution frequency of the change in H3K27ac occupancy in UCH1 cells in response to KDOBA67 versus DMSO control as assessed by ChIP-Rx and at the promoter of genes that are upregulated, downregulated, or unchanged in response to KDOBA67 as assessed by RNA-seq. The three distributions are statistically different one from another by Kolmogorov–Smirnov test ($P < 10^{-16}$). ***, $P \le 0.001$; ****, $P \le 0.0001$.

specific gamma-glutamylcyclotransferase 1 (*CHAC1*; **Fig. 2A–C**; Supplementary Fig. S4B–S4E), consistent with the antiproliferative results of H3K27 demethylase inhibitors (**Fig. 1**). Treatment of primary chordoma cultures with KDOBA67 revealed a similar transcriptional response to that seen in chordoma cell lines, including increases in ATF4/DDIT3-target genes (**Fig. 2D**).

H3K27 demethylase inhibition leads to genome-wide alteration of histone marks

We next investigated the mechanism by which KDOBA67 alters cellular gene expression. Using ChIP-sequencing, normalized with an exogenous reference genome (ChIP-Rx), we found that treatment of UCH1 cells with KDOBA67 increased H3K27me3 at TSS and gene bodies across the genome after 48 hours (**Fig. 2E**; Supplementary Fig. S4F). Pathway analysis revealed that differentially bound H3K27me3 peaks were at genes involved in chordoma cell biology, related to extracellular matrix organization, cell contact, and signaling (Supplementary Fig. S4G and Supplementary Dataset S3). ChIP-Rx also revealed a corresponding global decrease in H3K27ac at TSS (**Fig. 2E**; Supplementary Fig. S4H). To explore the wider effect of the increase in H3K27me3 on chromatin structure, we measured changes in the activating histone marks H3K9ac and H3K4me3 following KDOBA67 treatment and found a global decrease at TSS, similar to that seen for H3K27ac (**Fig. 2E**; Supplementary Fig. S4I and S4J). We then asked how the global loss of active histone marks in response to KDOBA67 treatment relates to the changes in gene expression. Plotting H3K27ac at the TSS of differentially expressed genes revealed that downregulated genes exhibited the greatest loss of H3K27ac (**Fig. 2F**). Thus, we conclude that inhibition of H3K27 demethylation leads to depletion of H3K27ac and inhibition of gene expression.

We next examined the effect on H3K4me3. As reported previously for GSK-J4 (42) we found that KDOBA67 exerts some inhibitory activity in non–cell-based assays against recombinantly expressed and purified KDM5 (JARID1) enzymes, the principal H3K4me3 demethylases (Supplementary Table S2). The decrease in H3K4me3 levels observed following treatment with KDOBA67 (**Fig. 2E**) is in stark contrast to the previously reported global increase in H3K4me3 following treatment with specific H3K4me3 demethylase inhibitors (43, 44) and indicates that the phenotype observed in our experiments is not an off-target effect against KDM5 enzymes.

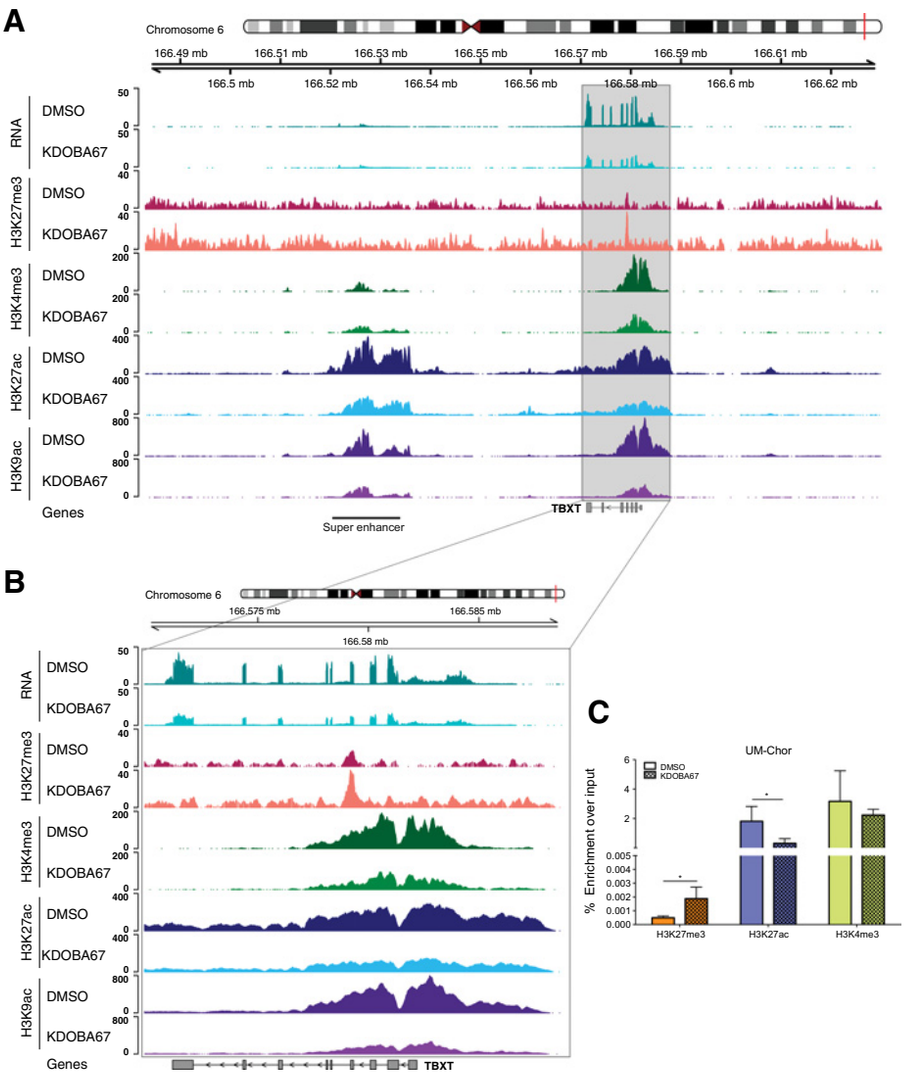

Figure 3.
Inhibition of H3K27 lysine demethylase leads to chromatin changes around *TBXT* in chordoma. **A,** RNA expression (top pair of tracks), H3K27me3, H3K4me3, H3K27ac, and H3K9ac modifications at the *TBXT* locus in UCH1 cells treated with KDOBA67 (light colors) or DMSO (dark colors) for 48 hours. An increase in the level of H3K27me3 over the gene locus is observed, with a concurrent decrease in the levels of H3K27ac, H3K9ac, and H3K4me3 at the *TBXT* promoter and superenhancer (labeled). Tracks show the average of replicates. **B,** As in **A** but with an expanded view of the *TBXT* gene. **C,** H3K27me3, H3K27ac, and H3K4me3 enrichment at the *TBXT* promoter (−2 Kb from the TSS) in UM-Chor cells treated with KDOBA67 or DMSO for 48 hours, assessed by ChIP-qPCR. Results from four biological replicates per condition. ChIP-qPCR data for positive control sites are shown in Supplementary Fig. S4K–S4M. *, $P < 0.05$.

H3K27 demethylase inhibition alters chromatin state at *TBXT* and inhibits its expression

Given the central role of TBXT in the pathogenesis of chordoma (20, 23), in addition to the evidence that silencing H3K27 demethylases in development represses *TBXT* expression (10, 11), we next asked whether inhibition of KDM6A/B suppressed *TBXT* in chordoma cell lines. Treatment with KDOBA67 led to an increase in H3K27me3 and a decrease in H3K27ac, H3K9ac, and H3K4me3 at the *TBXT* gene locus in the UCH1 cell line (**Fig. 3A** and **B**), which was associated with significantly reduced expression of *TBXT* as measured by RNA-seq (**Fig. 3A** and **B**, top pair of tracks, and Supplementary Dataset S2). These chromatin alterations were confirmed in UM-Chor cells using ChIP-qPCR (**Fig. 3C**; Supplementary Fig. S4K–S4M). H3K27ac was also significantly reduced at the recently identified *TBXT*-associated superenhancer and active regulatory region (**Fig. 3A**; Supplementary Fig. S5A and S5B; ref. 29).

Western blot and qRT-PCR analyses confirmed that treatment with either GSK-J4 or KDOBA67, but not with the control compound GSK-J5, also reduced *TBXT* expression in two other chordoma cell lines (**Fig. 4A** and **B**), including MUG-Chor cells that harbor multiple copies of *TBXT* (www.chordomafoundation.org). The relevance of KDM6A/B inhibition for disease was further supported by the reduction in cell proliferation (**Fig. 4C**) and *TBXT* expression (**Fig. 4D**) following *in vitro* treatment of patient-derived primary chordoma samples with KDOBA67. The reduction of *TBXT* expression was reproduced by CRISPR/Cas9-mediated knockout of *KDM6A/B* in both UCH1 and UM-Chor cell lines, demonstrating this to be a direct effect of the compound on these enzymes (**Fig. 4E**; Supplementary Fig. S5C).

Histone modifications directly control *TBXT* expression in chordoma

Next, we tested if KDM6A/B directly targets the *TBXT* locus. ChIP-qPCR revealed binding of both KDM6A and KDM6B at the *TBXT* superenhancer and promoter regions in the UCH1 cell line (**Fig. 5A**). In contrast, lower levels of KDM6A/B were found at the promoter of homeobox A7 (*HOXA7)*, a known polycomb target (**Fig. 5A**). The binding of KDM6A/B was not altered at either the *TBXT* or *HOXA7* promoter regions in response to KDOBA67 treatment, implying that this compound specifically acts to inhibit the catalytic activity of demethylases rather than altering their recruitment to chromatin (**Fig. 5B**).

We next asked whether variations in H3K27me3 and other histone marks could explain the difference in expression of *TBXT* in chordoma cells and other mesoderm-derived cancer cells in which physiologic silencing of *TBXT* occurs during development. ChIP-qPCR revealed that the repressive marks H3K27me3 and H3K9me2 were enriched at the *TBXT* promoter region in the osteosarcoma U2OS cell line but not in the chordoma lines tested (**Fig. 5C**), consistent with the expression of *TBXT* in chordoma but not in osteosarcoma. Reciprocally, enrichment of H3K4me3 and H3.3, both associated with active gene transcription, was restricted to chordoma cells (**Fig. 5C**).

We next investigated whether DNA methylation contributes to the regulation of *TBXT* expression in chordomas in view of the evidence that it cooperates with histone modifications to regulate *TBXT* expression in development (8). We found low levels of DNA methylation in the promoter region and at the TSS of *TBXT* in primary chordoma tumors and also in bone tumors that do not express *TBXT* (**Fig. 5D**; Supplementary Fig. S6). Taken together, these data support the concept that *TBXT* expression is regulated by histone modification and not by DNA promoter methylation.

H3K27 demethylases inhibition targets TBXT and induces chordoma cell death

In addition to suppression of *TBXT* in response to treatment with KDOBA67, we noted activation of an ATF4 stress–induced pathway (**Fig. 2**; ref. 45). Below we provide four lines of evidence showing that the antiproliferative effect mediated by KDM6 inhibitors is largely related to the reduction in *TBXT* expression rather than activation of the ATF4 pathway.

First, having established that *TBXT* is a KDM6A/B target gene (**Fig. 5A** and **B**), we asked whether the reduction in *TBXT* gene expression was a direct consequence of KDM6A/B inhibition or an event secondary to induced metabolic stress. Measuring the effect of KDOBA67 on nascent gene transcription, we found that the *TBXT* pre-mRNA was reduced as early as 3 hours after exposure to KDOBA67 (**Fig. 6A**). Furthermore, time course experiments in three chordoma cell lines demonstrated that *TBXT* expression decreased prior to upregulation of genes associated with the ATF4 response (**Fig. 6B**; Supplementary Fig. S7A and S7B).

Second, we treated chordoma cells with ISRIB, a specific compound that inhibits the induction of the ATF4 response by interfering with eIF2α phosphorylation (46). ISRIB treatment significantly reduced the expression of ATF4 and ATF4-target genes (*INHBE* and *DDIT3*) but did not prevent KDOBA67-induced downregulation of *TBXT* (**Fig. 6C**; Supplementary Fig. S7C–S7E) nor the reduction in cell proliferation (**Fig. 6D**; Supplementary Fig. S7F and S7G).

Third, analysis of the transcriptional profile of UCH1 in response to KDOBA67 treatment revealed that, together with *TBXT*, genes encoding transcription factors directly targeted by TBXT, such as the SRY-Box transcription factor 5 (*SOX5;* refs. 20, 47), or predicted to be targeted by TBXT, such as PBX homeobox 1 (*PBX1)* and NK homeobox 6–1 *(NKX6–1)*, were downregulated (**Fig. 2A**; Supplementary Fig. S4B–S4E). Furthermore, experimentally validated *TBXT* target genes (20) were significantly enriched among those genes altered in response to KDOBA67 (**Fig. 6E**), indicating that KDM6A/B inhibition results in the repression of a TBXT-controlled transcriptional network. Indeed, the antiproliferative effect of KDM6 inhibition is also phenocopied by CRISPR/Cas9-mediated knockout of *TBXT* (Supplementary Fig. S7H–S7J).

Finally, to determine whether repression of *TBXT* expression was necessary for KDOBA67-induced cell death, we overexpressed hemagglutinin-tagged TBXT (TBXT-HA) in the human chordoma cell line UCH1 under a strong promoter, which, unlike the endogenous regulatory elements, was not sensitive to KDM6A/B inhibition (**Fig. 6F** and **G**; Supplementary Fig. S7K and S7L). We found that ectopic expression of TBXT-HA partially rescued KDOBA67-induced cell death (**Fig. 6G** and **H**).

Discussion

The number of small-molecule inhibitors that have been found to induce significant antiproliferative effects in chordoma cells is limited (29, 30, 48). Here, we show that H3K27 demethylase inhibitors suppress cell viability and *TBXT* expression in multiple human chordoma cell lines as well as patient-derived primary chordoma samples. This is in striking contrast to previous studies that reported that EGFR inhibitors decrease chordoma cell viability to a variable degree across only some chordoma cell lines, and reduction of *TBXT* expression was only seen in response to a single compound, afatinib (30, 48, 49).

Our finding that KDM6A/B inhibition increases H3K27me3 at the *TBXT* locus demonstrates that it is feasible to block the function of

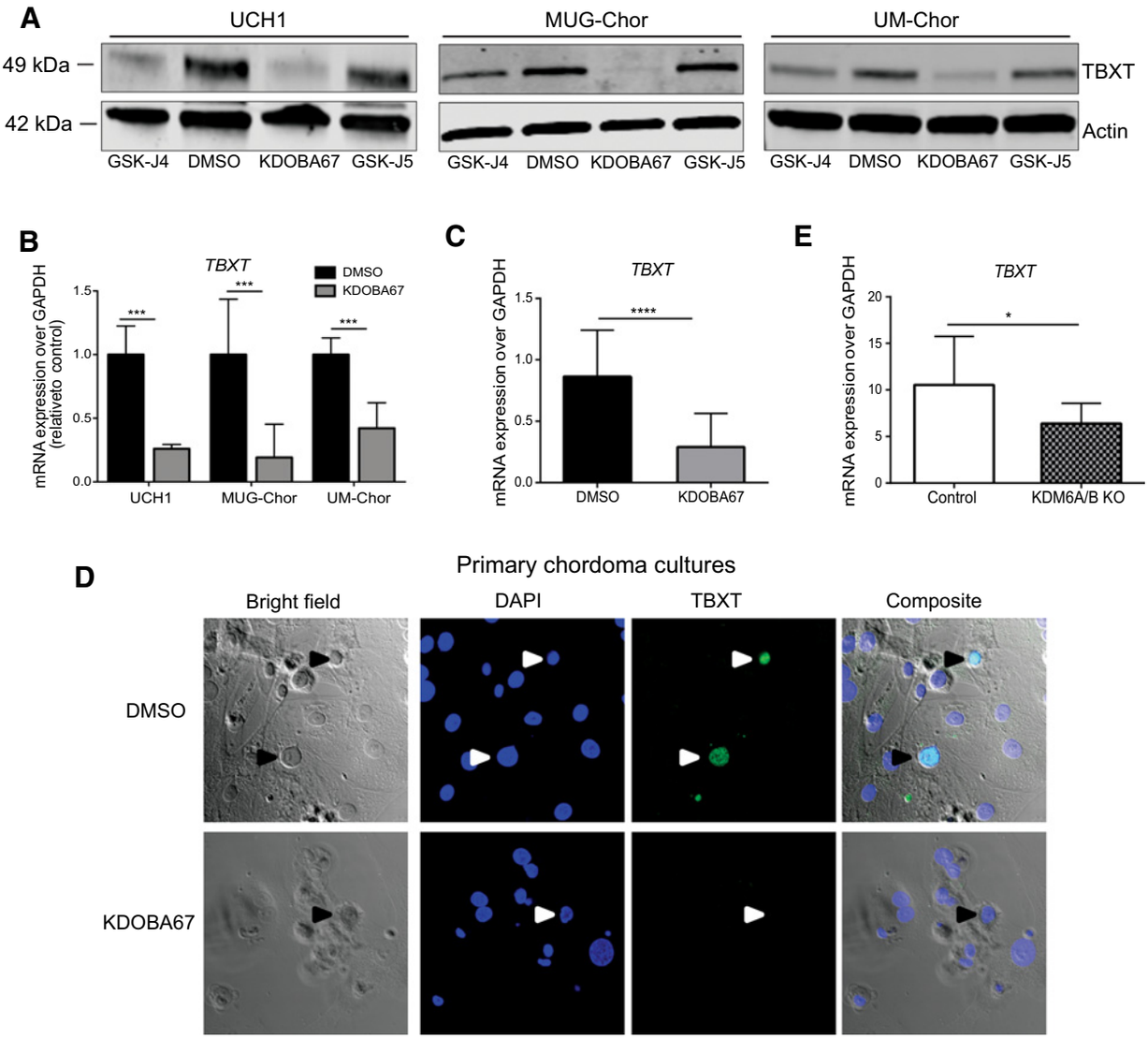

Figure 4.

Inhibition of H3K27 lysine demethylase leads to inactivation of TBXT in chordoma. **A,** Protein expression of *TBXT* in chordoma cell lines following treatment with KDOBA67 for 48 hours as assessed by Western blotting. β-Actin was used as an endogenous control. Representative blots of two independent experiments. **B,** *TBXT* expression in UCH1, MUG-Chor, and UM-Chor following KDOBA67 treatment for 48 hours, as assessed by qRT-PCR in three independent experiments with three biological replicates per condition per cell line. **C,** *TBXT* transcript level was reduced in primary chordoma cultures treated with KDOBA67 for 6 days, as assessed by qPCR. $N = 4$ primary samples, at least three replicates per condition per sample. **D,** Cell death and reduction in expression of TBXT (arrowheads) as shown by immunofluorescence in KDOBA67- and DMSO-treated patient-derived chordoma cultures for 6 days. TBXT-positive chordoma cells are interspersed between tumor-derived stromal cells. TBXT, green; DAPI, blue. Magnification, ×40. Representative pictures from one sample; experiment performed on two samples. **E,** Expression of *TBXT* was reduced in UCH1 following double KO of *KDM6A/B*, assessed by qPCR. Quantification of two independent experiments, with two biological replicates per condition per experiment. *, $P \leq 0.05$; ***, $P \leq 0.001$; ****, $P \leq 0.0001$.

TBXT in chordoma cells by manipulating its chromatin environment. Such a strategy has been demonstrated successfully for oncogenes in other malignancies, for example repression of c-Myc with bromodomain and extra terminal domain protein inhibitors such as JQ1 in multiple myeloma (26), thereby circumventing the challenge of directly inhibiting transcription factors, which are often considered "undruggable" (50). Moreover, our previous work on human immune cell types such as macrophages, natural killer, or T cells (28, 39, 51) demonstrates reversible antiproliferative and anti-inflammatory effects upon GSK-J4 inhibition without signs of cell death, suggesting selective proapoptotic effects on cancer cells. This supports the concept that H3K27 demethylase inhibitors could potentially be used in the treatment of more common cancers that show a dependency on *TBXT* expression (18). However, KDM6 inhibitor tool compounds such as GSK-J4 and KDOBA67 have been developed as *ex vivo* tool compounds (41) and require significant chemical optimization to reach adequate pharmacokinetic and metabolic properties to justify *in vivo* studies. Although GSK-J1 is a potent *in vitro* tool compound, its carboxylate structure significantly impairs cellular uptake. The ethyl ester derivative GSK-J4 requires intracellular esterases for release of

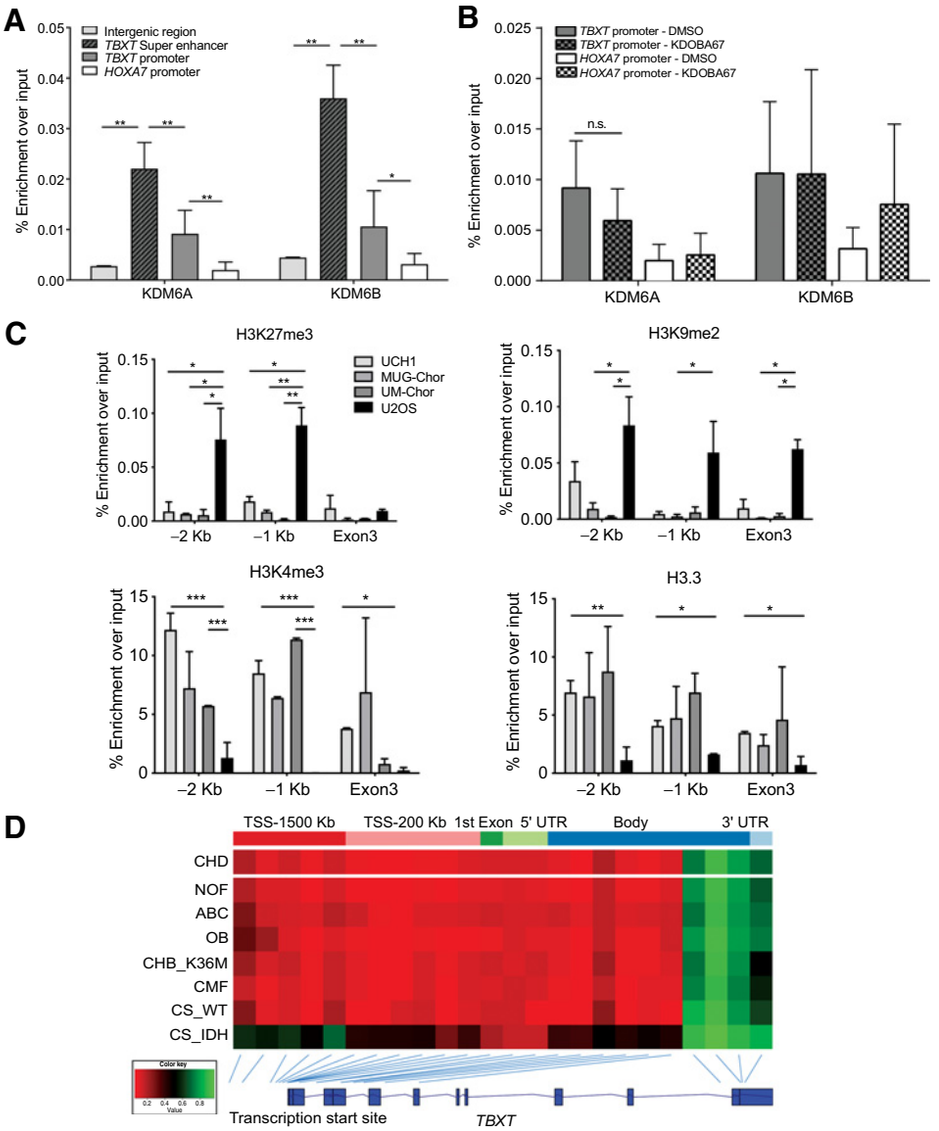

Figure 5.

Histone modifiers epigenetically control TBXT expression in chordoma. **A,** ChIP-qPCR of KDM6A and KDM6B occupancy in UCH1 cells at the *TBXT* superenhancer (indicated in **Fig. 3A**), *TBXT* and *HOXA7* promoter (-1 Kb from TSS), and a control intergenic region (300 Kb downstream of *TBXT*). Four biological replicates per condition. **B,** ChIP-qPCR of KDM6A and KDM6B at the *TBXT* or *HOXA7* promoter (-1 Kb from TSS) in UCH1 cells treated with KDOBA67 or DMSO for 48 hours. Two biological replicates per condition per experiment, two independent experiments. **C,** ChIP-PCR of H3K27me3 and H3K9me3 (top), H3K4me3 and H3.3 (bottom) in three chordoma cell lines (UCH1, MUG-Chor, UM-Chor), and the osteosarcoma cell line U2OS. Two independent experiments, with three biological replicates per condition per experiment. **D,** The DNA at the promoter region of *TBXT* is hypomethylated in all primary human chordomas ($n = 35$) and in other mesenchymal tumors not associated with the expression of *TBXT*. From top, chordoma, nonossifying fibroma ($n = 12$), aneurysmal bone cysts ($n = 9$), osteoblastoma ($n = 12$), chondroblastoma harboring H3.3-K36M mutation ($n = 17$), chondromyxoid fibroma ($n = 25$), chondrosarcoma WT ($n = 2$), chondrosarcoma harboring an IDH mutant ($n = 3$). The average beta value for each probe is plotted with the position of the probe shown relative to the *TBXT* gene body. *, $P \le 0.05$; **, $P \le 0.01$; ***, $P \le 0.001$.

GSK-J1: this allows cellular uptake in most cell culture experiments but its *in vivo* use is significantly hampered by the activity of unspecific serum hydrolases. This renders the compound metabolically unstable, requiring unsuitably high dosing in order to reach sufficient *in vivo* exposure levels.

H3K27me3 is deposited at promoter regions by PRC2 and allows recruitment of canonical CBX-containing forms of PRC1, and further recruitment of PRC2, thus reinforcing polycomb activity at target sites (14, 15). Ectopic expression of KDM6B has previously been shown to lead to a marked decrease of H3K27me3 and delocalization of Polycomb proteins *in vivo* (52), consistent with our observations that KDM6A/B inhibition causes a global increase in H3K27me3. The increase in H3K27me3 across the genome, even at genes at which H3K27me3 is not normally detected, is consistent with the chromatin sampling model for PRC2 recruitment (53). The identified concomitant global decrease in H3K27ac is consistent with the known antagonistic relationship between H3K27 methylation and acetylation (12, 13). Previous work suggests that the Mixed Lineage Leukemia/Complex of Protein-Associated with Set1 (MLL/COMPASS)-like complex 4 (MLL4), which contains KDM6A, is involved in enhancer H3K4 monomethylation and H3K27 acetylation through the recruitment of the acetyltransferase p300 in murine ESCs (54). MLL4 also establishes H3K4me3 and activates superenhancers at tumor-suppressor genes (55) and at genes that drive cellular differentiation (56). Although the role of KDM6A in enhancer activation might not solely rely on its enzymatic function, its presence in MLL4 may explain the global reduction in H3K4me3 and H3K27ac levels in chordoma cells following loss of KDM6A function, a phenomenon reported also in pancreatic cancer (57).

Our study provides new insights into the function of H3K27 demethylases in tumor biology. KDM6 enzymes can act in a cancer type–specific manner as oncogenes or tumor suppressors, but only mutations in KDM6A have thus far been identified. KDM6 enzymes are ubiquitously expressed, suggesting "housekeeping" functions in maintaining H3K27 methylation levels. In addition, KDM6B is highly and transiently induced by various stimuli (such as cytokines or growth factors) to modulate the temporal expression of key genes in lineage development and inflammation (58). We show here that

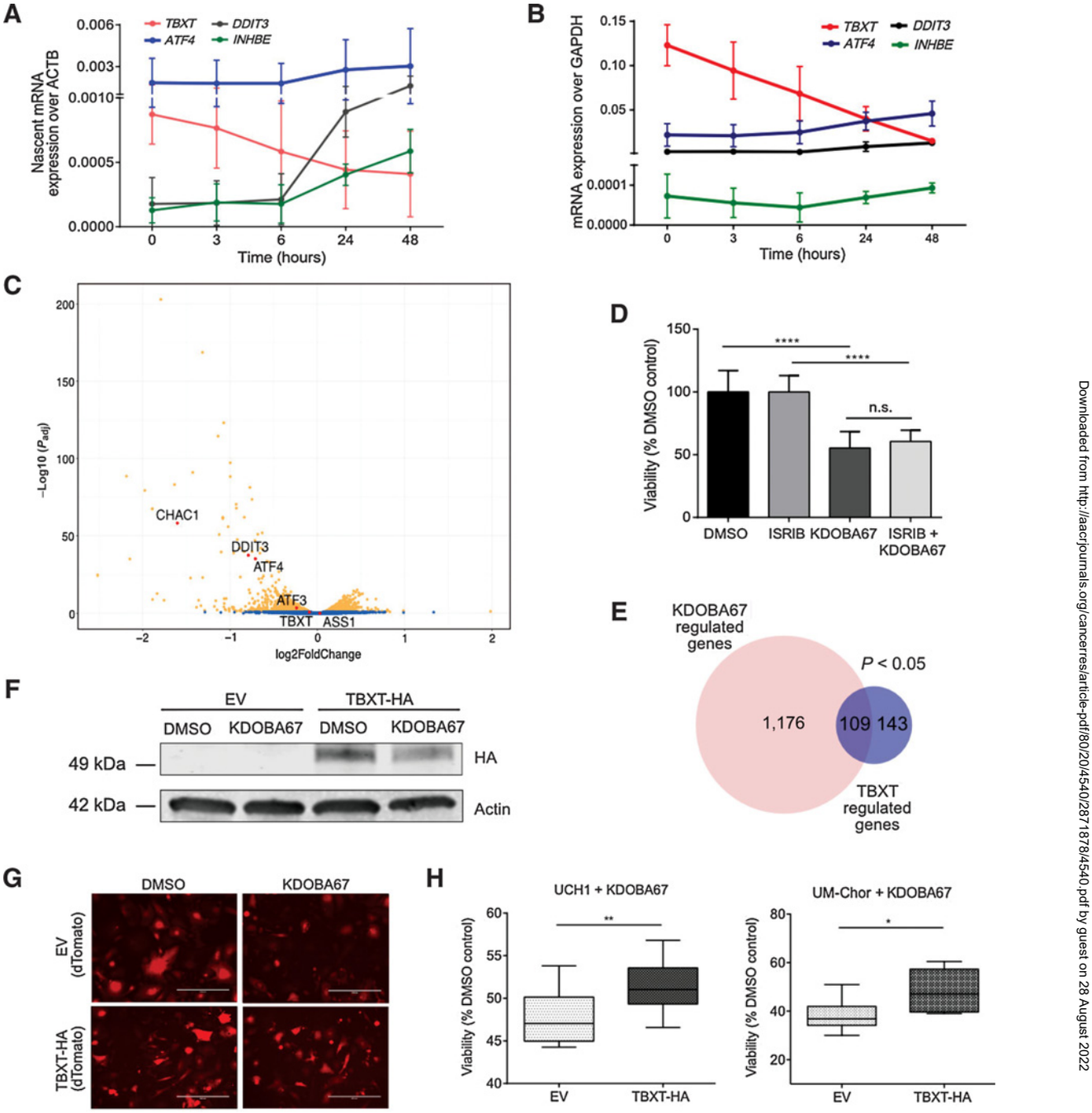

Figure 6.

Epigenetic regulation of *TBXT* occurs independently of an ATF4-stress response and is key to the lethality induced by H3K27 demethylase inhibitors. **A** and **B,** *ATF4, DDIT3, INHBE,* and *TBXT* regulation over a time course in response to KDOBA67 in UCH1, by qPCR of nascent RNA (**A**) and total RNA (**B**). Two independent experiments, three replicates per condition each experiment. Results for total RNA for UM-Chor and MUG-Chor are reported in Supplementary Fig. S7. **C,** Volcano plot summarizing differential gene expression by RNA-seq in UCH1 cells treated with KDOBA67 for 48 hours in the presence or absence of ISRIB. Blue, not significant; orange, $P_{adj} < 0.05$. Three biological replicates. **D,** Proliferation of UCH1 cells in response to treatment with KDOBA67 for 48 hours in the presence or absence of ISRIB. Three independent experiments, three replicates per condition per experiment. **E,** Venn diagram showing the number of genes regulated by KDOBA67 treatment in UCH1 cells (by RNA-seq; **Fig. 2**) that overlap with genes previously identified as direct targets of TBXT in UCH1 cells using ChIP-seq in ref. 20. **F,** Overexpression of TBXT-HA in UCH1 cells is not affected by KDOBA67 treatment; similar levels of HA by Western blot in cells treated with KDOBA67 or DMSO. **G,** Overexpression of TBXT-HA or control EV in UCH1 cells is achieved in >95% of cells; expression of dTomato by fluorescence microscopy of EV and TBXT-HA cells treated with KDOBA67 or DMSO (representative images; scale bar, 400 μm). **H,** Overexpression of TBXT-HA mitigates the reduction in cell viability in response to treatment with KDOBA67 for 4 days in UCH1 and UM-Chor. Four replicates per condition in three (UCH1) and two (UM-Chor) independent experiments. *, $P \le 0.05$; **, $P \le 0.01$; ****, $P \le 0.0001$; n.s., nonsignificant.

inhibition/knockdown of both KDM6 enzymes is necessary to obtain an antiproliferative effect, suggesting a cooperative role of KDM6 enzymes in the installation of global methylation patterns.

This research reveals that treatment with H3K27 demethylases inhibitors alters a network of genes similar to those altered by knocking down *TBXT* in chordoma cells, including genes involved in the cell cycle, production of extracellular matrix, growth factor, and cytokine secretion, which are necessary for the survival of chordoma cells (20) and pertinent to notochord formation (20, 30). Moreover, in keeping with our previous studies and that of others (28, 39, 51), we describe the activation of an ATF4- and DDIT3-driven stress response, thereby identifying this pathway as an additional possible therapeutic option for chordoma (45). However, our data suggest that the effect of H3K27me3 demethylase inhibitors on chordoma cell growth is primarily mediated by suppression of *TBXT* expression rather than activation of the ATF4 metabolic stress response. Our finding that the effect of KDOBA67 treatment on cell death was not fully reversed by *TBXT* overexpression is likely to be explained by the substantial number of genes, which, in addition to *TBXT*, are also repressed in response to KDOBA67. These genes include both direct and/or indirect targets of TBXT.

In conclusion, our study shows that inactivation of H3K27 demethylases alters the expression of genes critical to the survival of chordoma cancer cells and opens the door to further studies investigating how KDM6A/B can be exploited as potential therapeutic targets.

Disclosure of Potential Conflicts of Interest

T. Szommer reports grants from Innovative Medicine Initiative and grants from Wellcome during the conduct of the study. P.E. Brennan reports grants from Innovative Medicines Initiative and grants from Wellcome during the conduct of the study. R.G. Jenner reports grants from Medical Research Council during the conduct of the study. U. Oppermann reports grants from Chordoma Foundation, Bone Cancer Research Trust, Rosetrees Trust, CRUK, and Leducq Foundation. No potential conflicts of interest were disclosed by the other authors.

Authors' Contributions

L. Cottone: Conceptualization, investigation, writing-original draft, writing-review and editing. **A.P. Cribbs:** Data curation, formal analysis. **G. Khandelwal:** Data curation, formal analysis. **G. Wells:** Investigation. **L. Ligammari:** Investigation. **M. Philpott:** Investigation. **A. Tumber:** Resources. **P. Lombard:** Data curation, formal analysis. **E.S. Hookway:** Formal analysis, investigation. **T. Szommer:** Resources. **C. Johansson:** Resources. **P.E. Brennan:** Resources. **N. Pillay:** Formal analysis, writing-original draft. **R.G. Jenner:** Formal analysis, writing-original draft, writing-review and editing. **U. Oppermann:** Conceptualization, formal analysis, supervision, funding acquisition, writing-original draft, writing-review and editing. **A.M. Flanagan:** Conceptualization, supervision, funding acquisition, writing-original draft, writing-review and editing.

Acknowledgments

Funding for this project was received from the Chordoma Foundation (A.M. Flanagan and U. Oppermann), Chordoma UK (A.M. Flanagan), Sarcoma UK (A.M. Flanagan and U. Oppermann), Bone Cancer Research Trust (A.P. Cribbs, L. Cottone, A.M. Flanagan, and U. Oppermann), Rosetrees Trust (M46-F1 to A.M. Flanagan), CRUK (A23900 to U. Oppermann), the LEAN program grant of the Leducq Foundation (U. Oppermann), the Oxford NIHR Biomedical Research Centre, Skeletal Cancer Action Trust (A.M. Flanagan), a RNOH NHS R&D grant (A.M. Flanagan), and the People Programme (Marie Curie Actions) of the European Union's Seventh Framework Programme (FP7/2007-2013 to U. Oppermann) under REA grant agreement no. 609305. A.M. Flanagan is a National Institute for Health Research (NIHR) senior investigator. N. Pillay is a CRUK clinician scientist (grant no. 18387). L. Cottone, R.G. Jenner, A.M. Flanagan, and N. Pillay are supported by NIHR, UCLH Biomedical Research Centre, and the Cancer Research Experimental Cancer Centre. G. Khandelwal is supported by the CRUK UCL Centre and an MRC grant to R.G. Jenner (MR/R001413/1). The SGC is a registered charity (number 1097737) that receives funds from AbbVie, Bayer Pharma AG, Boehringer Ingelheim, Canada Foundation for Innovation, Eshelman Institute for Innovation, Genome Canada, Innovative Medicines Initiative (EU/EFPIA; ULTRA-DD grant no. 115766), Janssen, MSD, Merck KGaA, Novartis Pharma AG, Ontario Ministry of Economic Development and Innovation, Pfizer, São Paulo Research Foundation-FAPESP, Takeda, and Wellcome (106169/ZZ14/Z).

We thank Carina Gileadi and Kannan Velupillai for performing crystallization experiments with KDOBA67 and UTY. We thank Drs. Ivana Bjedov and Victoria Martinez Miguel, UCL Cancer Institute, for providing S2 *Drosophila* cells and Donna Magsumbol for technical support. We thank Professor Paolo Salomoni, Dr. Andy Feber, Dr. Teresa Sposito, Dr. Stanimir Dulev, Dr. Christopher Steele, Dr. Manuel Beltran Nebot, and Dr. Javier Herrero for their valuable discussion and input, and UCL Cancer Institute Core Facilities, the Biobank Team at the RNOH, and the healthcare workers who care for the patients. We thank the patients for the generous donation of their material without which this research would not have been feasible.

The costs of publication of this article were defrayed in part by the payment of page charges. This article must therefore be hereby marked *advertisement* in accordance with 18 U.S.C. Section 1734 solely to indicate this fact.

Received April 25, 2020; revised July 8, 2020; accepted August 19, 2020; published first August 27, 2020.

References

1. Mikkelsen TS, Ku M, Jaffe DB, Issac B, Lieberman E, Giannoukos G, et al. Genome-wide maps of chromatin state in pluripotent and lineage-committed cells. Nature 2007;448:553–60.
2. Mallo M, Alonso CR. The regulation of Hox gene expression during animal development. Development 2013;140:3951–63.
3. Flavahan WA, Gaskell E, Bernstein BE. Epigenetic plasticity and the hallmarks of cancer. Science 2017;357:eaal2380.
4. Cerdan C, McIntyre BAS, Mechael R, Levadoux-Martin M, Yang J, Lee JB, et al. Activin A promotes hematopoietic fated mesoderm development through upregulation of brachyury in human embryonic stem cells. Stem Cells Dev 2012;21:2866–77.
5. Wilkinson DG, Bhatt S, Herrmann BG. Expression pattern of the mouse T gene and its role in mesoderm formation. Nature 1990;343:657–9.
6. Risbud MV, Shapiro IM. Notochordal cells in the adult intervertebral disc: New perspective on an old question. Crit Rev Eukaryot Gene Expr 2011;21:29–41.
7. Lyu J, Jho E, Lu W. Smek promotes histone deacetylation to suppress transcription of Wnt target gene brachyury in pluripotent embryonic stem cells. Cell Res 2011;21:911–21.
8. Dansranjavin T, Krehl S, Mueller T, Mueller LP, Schmoll HJ, Dammann RH. The role of promoter CpG methylation in the epigenetic control of stem cell related genes during differentiation. Cell Cycle 2009;8:916–24.
9. Schmidt CS, Bultmann S, Meilinger D, Zacher B, Tresch A, Maier KC, et al. Global DNA hypomethylation prevents consolidation of differentiation programs and allows reversion to the embryonic stem cell state. PLoS One 2012;7:e52629.
10. Naruse C, Shibata S, Tamura M, Kawaguchi T, Abe K, Sugihara K, et al. New insights into the role of Jmjd3 and Utx in axial skeletal formation in mice. FASEB J 2017;31:2252–66.
11. Morales Torres C, Laugesen A, Helin K. Utx is required for proper induction of ectoderm and mesoderm during differentiation of embryonic stem cells. PLoS One 2013;8:1–15.
12. Pasini D, Malatesta M, Jung HR, Walfridsson J, Willer A, Olsson L, et al. Characterization of an antagonistic switch between histone H3 lysine 27 methylation and acetylation in the transcriptional regulation of Polycomb group target genes. Nucleic Acids Res 2010;38:4958–69.
13. Lavarone E, Barbieri CM, Pasini D. Dissecting the role of H3K27 acetylation and methylation in PRC2 mediated control of cellular identity. Nat Commun Springer US; 2019;10:1–16.
14. Schuettengruber B, Bourbon HM, Di Croce L, Cavalli G. Genome regulation by Polycomb and Trithorax: 70 years and counting. Cell 2017;171:34–57.

15. Comet I, Riising EM, Leblanc B, Helin K. Maintaining cell identity: PRC2-mediated regulation of transcription and cancer. Nat Rev Cancer 2016;16:803–10.
16. WHO Classification of Tumours Editorial Board. Notochordal tumours. In: WHO classification of soft tissue and bone tumours. Eds., CDM Fletcher, JA Bridge, PCW Hogandoom, F Mertens. Lyon, France: IARC; 2020. p. 449–57.
17. Vujovic S, Henderson S, Presneau N, Odell E, Jacques TS, Tirabosco R, et al. Brachyury, a crucial regulator of notochordal development, is a novel biomarker for chordomas. J Pathol 2006;209:157–65.
18. Hamilton DH, David JM, Dominguez C, Palena C. Development of cancer vaccines targeting brachyury, a transcription factor associated with tumor epithelial-mesenchymal transition. Cells Tissues Organs 2017;203:128–38.
19. Miettinen M, Wang Z, Lasota J, Heery C, Schlom J, Palena C. Nuclear brachyury expression is consistent in chordoma, common in germ cell tumors and small cell carcinomas, and rare in other carcinomas and sarcomas: an immunohistochemical study of 5229 cases. Am J Surg Pathol 2015;39:1305–12.
20. Nelson AC, Pillay N, Henderson S, Presneau N, Tirabosco R, Halai D, et al. An integrated functional genomics approach identifies the regulatory network directed by brachyury (T) in chordoma. J Pathol 2012;228:274–85.
21. Yang XR, Ng D, Alcorta DA, Liebsch NJ, Sheridan E, Li S, et al. T (brachyury) gene duplication confers major susceptibility to familial chordoma. Nat Genet 2009;41:1176–8.
22. Tarpey PS, Behjati S, Young MD, Martincorena I, Alexandrov LB, Farndon SJ, et al. The driver landscape of sporadic chordoma. Nat Commun 2017;8:890.
23. Presneau N, Shalaby A, Ye H, Pillay N, Halai D, Idowu B, et al. Role of the transcription factor T (brachyury) in the pathogenesis of sporadic chordoma: a genetic and functional-based study. J Pathol 2011;223:327–35.
24. Hsu W, Mohyeldin A, Shah SR, ap Rhys CM, Johnson LF, Sedora-Roman NI, et al. Generation of chordoma cell line JHC7 and the identification of Brachyury as a novel molecular target. J Neurosurg 2011;115:760–9.
25. Momparler RL, Bouchard J, Onetto N, Rivard GE. 5-AZA-2′-deoxycytidine therapy in patients with acute leukemia inhibits DNA methylation. Leuk Res 1984;8:181–5.
26. Delmore JE, Issa GC, Lemieux ME, Rahl PB, Shi J, Jacobs HM, et al. BET bromodomain inhibition as a therapeutic strategy to target c-Myc. Cell 2011;146:904–17.
27. Hashizume R, Andor N, Ihara Y, Lerner R, Gan H, Chen X, et al. Pharmacologic inhibition of histone demethylation as a therapy for pediatric brainstem glioma. Nat Med 2014;20:1394–6.
28. Lochmann TL, Powell KM, Ham J, Floros KV. Heisey DAR, Kurupi RIJ, et al. Targeted inhibition of histone H3K27 demethylation is effective in high-risk neuroblastoma. Sci Transl Med 2018;10:1–13.
29. Sharifnia T, Wawer MJ, Chen T, Huang QY, Weir BA, Sizemore A, et al. Small-molecule targeting of brachyury transcription factor addiction in chordoma. Nat Med 2019;25:292–300.
30. Scheipl S, Barnard M, Cottone L, Jorgensen M, Drewry DH, Zuercher WJ, et al. EGFR inhibitors identified as a potential treatment for chordoma in a focused compound screen. J Pathol 2016;239:320–34.
31. Lampada A, O'Prey J, Szabadkai G, Ryan KM, Hochhauser D, Salomoni P. MTORC1-independent autophagy regulates receptor tyrosine kinase phosphorylation in colorectal cancer cells via an mTORC2-mediated mechanism. Cell Death Differ 2017;24:1045–62.
32. Shalem O, Sanjana NE, Hartenian E, Shi X, Scott DA, Mikkelsen TS, et al. Genome-scale CRISPR-Cas9 knockout screening in human cells. Science 2014;343:84–7.
33. Sims D, Ilott NE, Sansom SN, Sudbery IM, Johnson JS, Fawcett KA, et al. Genome analysis CGAT: computational genomics analysis toolkit. 2014;30:1–2.
34. Pertea M, Kim D, Pertea GM, Leek JT, Salzberg SL. Transcript-level expression analysis of RNA-seq experiments with HISAT, StringTie and Ballgown. Nat Protoc 2016;11:1650–67.
35. Langmead B, Salzberg SL. Bowtie2. Nat Methods 2013;9:357–9.
36. Zang C, Schones DE, Zeng C, Cui K, Zhao K, Peng W. A clustering approach for identification of enriched domains from histone modification ChIP-Seq data. Bioinformatics 2009;25:1952–8.
37. Fursova NA, Blackledge NP, Nakayama M, Ito S, Koseki Y, Farcas AM, et al. Synergy between variant PRC1 complexes defines polycomb-mediated gene repression. Mol Cell 2019;74:1020–36.
38. Zhang Y, Liu T, Meyer CA, Eeckhoute J, Johnson DS, Bernstein BE, et al. Model-based analysis of ChIP-Seq (MACS). Genome Biol 2008;9:R137.
39. Cribbs A, Hookway ES, Wells G, Lindow M, Obad S, Oerum H, et al. Inhibition of histone H3K27 demethylases selectively modulates inflammatory phenotypes of natural killer cells. J Biol Chem 2018;293:2422–37.
40. Lee DH, Zhang Y, Kassam AB, Park MJ, Gardner P, Prevedello D, et al. Combined PDGFR and HDAC inhibition overcomes PTEN disruption in Chordoma. PLoS One 2015;10:e0134426.
41. Kruidenier L, Chung C, Cheng Z, Liddle J, Che K, Joberty G, et al. A selective jumonji H3K27 demethylase inhibitor modulates the proinflammatory macrophage response. Nature 2012;488:404–8.
42. Heinemann B, Nielsen JM, Hudlebusch HR, Lees MJ, Larsen DV, Boesen T, et al. Inhibition of demethylases by GSK-J1/J4. Nature 2014;514:E1–2.
43. Johansson C, Velupillai S, Tumber A, Szykowska A, Hookway ES, Nowak RP, et al. Structural analysis of human KDM5B guides histone demethylase inhibitor development. Nat Chem Biol 2016;12:78–80.
44. Tumber A, Nuzzi A, Hookway ES, Hatch SB, Velupillai S, Johansson C, et al. Potent and selective KDM5 inhibitor stops cellular demethylation of H3K4me3 at transcription start sites and proliferation of MM1S myeloma cells. Cell Chem Biol 2017;138:981–92.
45. Singleton DC, Harris AL. Targeting the ATF4 pathway in cancer therapy. Expert Opin Ther Targets 2012;16:1189–202.
46. Sidrauski C, McGeachy AM, Ingolia NT, Walter P. The small molecule ISRIB reverses the effects of eIF2α phosphorylation on translation and stress granule assembly. Elife 2015;4:e05033.
47. Smits P. Sox5 and Sox6 are required for notochord extracellular matrix sheath formation, notochord cell survival and development of the nucleus pulposus of intervertebral discs. Development 2003;130:1135–48.
48. Magnaghi P, Salom B, Cozzi L, Amboldi N, Ballinari D, Tamborini E, et al. Afatinib is a new therapeutic approach in chordoma with a unique ability to target EGFR and Brachyury. Mol Cancer Ther 2018;17:603–13.
49. Shalaby A, Presneau N, Ye H, Halai D, Berisha F, Idowu B, et al. The role of epidermal growth factor receptor in chordoma pathogenesis: a potential therapeutic target. J Pathol 2011;223:336–46.
50. Dang CV, Reddy EP, Shokat KM, Soucek L. Drugging the "undruggable" cancer targets. Nat Rev Cancer 2017;17:502–8.
51. Cribbs AP, Terlecki-Zaniewicz S, Philpott M, Baardman J, Ahern D, Lindow M, et al. Histone H3K27me3 demethylases regulate human Th17 cell development and effector functions by impacting on metabolism. Proc Natl Acad Sci U S A 2020;117:6056–66.
52. Agger K, Cloos PAC, Christensen J, Pasini D, Rose S, Rappsilber J, et al. UTX and JMJD3 are histone H3K27 demethylases involved in HOX gene regulation and development. Nature 2007;449:731–4.
53. Klose RJ, Cooper S, Farcas AM, Blackledge NP, Brockdorff N. Chromatin sampling-an emerging perspective on targeting polycomb repressor proteins. PLoS Genet 2013;9:e1003717.
54. Wang SP, Tang Z, Chen CW, Shimada M, Koche RP, Wang LH, et al. A UTX-MLL4-p300 transcriptional regulatory network coordinately shapes active enhancer landscapes for eliciting transcription. Mol Cell 2017;67:308–21.
55. Dhar SS, Zhao D, Lin T, Gu B, Pal K, Wu SJ, et al. MLL4 is required to maintain broad H3K4me3 peaks and super-enhancers at tumor suppressor genes. Mol Cell 2018;70:825–41.
56. Dhar SS, Lee SH, Kan PY, Voigt P, Ma L, Shi X, et al. Trans-tail regulation of MLL4-catalyzed H3K4 methylation by H4R3 symmetric dimethylation is mediated by a tandem PHD of MLL4. Genes Dev 2012;26:2749–62.
57. Watanabe S, Shimada S, Akiyama Y, Ishikawa Y, Ogura T, Ogawa K, et al. Loss of KDM6A characterizes a poor prognostic subtype of human pancreatic cancer and potentiates HDAC inhibitor lethality. Int J Cancer 2019;145:192–205.
58. Johansson C, Tumber A, Che K, Cain P, Nowak R, Gileadi C, et al. The roles of Jumonji-type oxygenases in human disease. Epigenomics 2014;6:89–120.